Pose Estimation of Mobile Robots with Quantized Measurements using EFIR Filtering: Experimental comparison with the EKF

Daniel Heß[a] and Christof Röhrig[a]

[a]University of Applied Sciences and Arts Dortmund, Germany *

Abstract

The unbiased finite impulse response (UFIR) filter is a universal estimator for linear systems. The extended UFIR (EFIR) is the counterpart of the UFIR for nonlinear systems and operates similarly to the well known extended Kalman filter (EKF). Pose estimation of mobile robots with quantized position measurements is an application, where the EKF leads to suboptimal accuracy. In this paper a pose estimator for quantized measurements based on the EFIR algorithm is developed. Experimental results conducted with a mobile robot on an array of floor installed RFID tags show that the proposed algorithm outperforms the quantized EKF in many cases.

1 Introduction

Along with the Kalman filter (KF), the unbiased finite impulse response (UFIR) filter is a universal linear estimator. The UFIR utilizes the most recent past measurements on a horizon of points and ignores the noise statistics of the dynamic system [1]. The KF is optimal only, if a system is linear and Gaussian and the noise statistics are known. Therefore the UFIR outperforms the KF in some practical applications, in which these requirements are not met [1].

Application of this research is the global localization of mobile robots using a grid of floor installed RFID tags. Global localization is the process of estimating position and heading (pose) of a mobile robot in Cartesian space without knowledge of the initial pose of the robot. A possible solution for global localization is the usage of auto-ID technology as artificial landmarks. Kiva Systems (now Amazon Robotics) uses 2D bar codes on the floor, which can be detected with a camera by the robots [2]. These bar codes specify the pathways and guarantee accurate localization. Drawbacks of this solution are the risk of polluting the bar codes and the need for predefined pathways, which restrict the movements of the robots.

Another possible solution for global localization is the usage of RFID technology as artificial landmarks. Passive RFID technology is often used in logistics and warehouse management for object identification and tracking. Typically the field of application is defined by the detection range of the RFID tags, which depends on the operation frequency. Usually LF or HF technology is used for self-localization of mobile systems (reader localization) and UHF technology is used for object identification in logistics applications [3].

The basic idea of using passive RFID tags as artificial landmarks for self-localization of mobile systems is not new.

Figure 1 Underlay with integrated RFID tags for localization of mobile robots

LF RFID tags are used to mark a predefined pathway for navigation of Automated Guided Vehicles (AGVs) in industry since more than two decades [4]. A known disadvantage of using LF RFID tags for vehicle navigation is the speed limitation of the vehicles caused by the low data transfer rate of LF tags. Also LF tags are comparatively expensive and the ground must be prepared with holes for these tags [5]. Owing to the cost of installation and material, the tags are installed on the pathway of the vehicles only.

An inexpensive and much more flexible option is the usage of a grid of floor installed standard HF RFID tags. This allows free navigation of vehicles without the need of predefined pathways. A commercially available product, which employs passive HF RFID tags in a floor is the NaviFloor® manufactured by Future-Shape. The NaviFloor® underlay is a glass fiber reinforcement in which passive HF RFID tags are embedded (see **Figure 1**). It is specially developed for installation beneath artificial flooring. Technical details of the NaviFloor® can be found in section 5.1.

This paper extends the work we have presented in [6, 7]. The main contribution of this paper is the development of

a novel localization algorithm, which fuses the information from RFID readings with odometry using the EFIR algorithm. The proposed algorithm requires a RFID reader with the only capability of detecting tags, no additional sensory information such as RSSI is required. We compare our localization algorithm based on EFIR filtering with the Quantized Kalman filter we have developed in [6, 7]. Experimental results show that the proposed algorithm outperforms the quantized EKF in many cases.

The rest of the paper is organized as follows: In section 2 the localization problem using floor installed RFID tags is defined. Section 3 presents related work. The compared localization algorithms are described in section 4. In section 5 the experimental setup including mobile robot and NaviFloor® is described. Experimental results are presented in section 6. Finally, the conclusions are given in section 7.

2   Problem Formulation

We consider the problem of localizing a mobile robot in a known environment. The mobile robot is equipped with a RFID reader and moves over a floor with n RFID tags. The position of the tags is known a priori. The robot moves in 2D space, the pose of the robot (position and heading) in the world frame is defined as $x = (x, y, \theta)^T$ in the configuration space (C-space) C, which is a subset of $\mathbb{R}^3$. $C = \mathbb{R}^2 \times S^1$ takes into account that $\theta \pm 2\pi$ yields to equivalent headings ($\theta \in [0, 2\pi)$). If a tag $T_i \in \{T_1, \ldots, T_n\}$ with position $t_i = (x_i, y_i)^T$ (defined in the world frame) is in range of the reader antenna, it is detected by the robot. The area where a tag can be detected by the reader is the detection area $\mathcal{A}$. The detection area can be described in the antenna frame, which is in a fixed position in the robot frame. Size and shape of $\mathcal{A}$ depend on the reader antenna, the tag type and the distance between them and is the same for all tags. The position of a tag in the antenna frame $z_i = (^A x_i, ^A y_i)^T$ can be described by

$$z_i = h(x, t_i), \qquad (1)$$

where x is the pose of the robot and t_i is the position of the tag T_i, both defined in the world frame. **Figure 2** shows
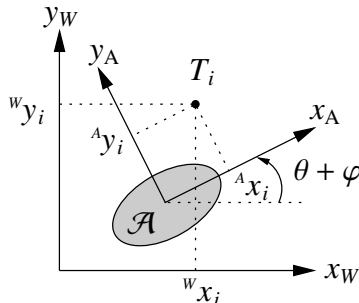

Figure 2 Position of RFID tag in world frame $(^W x_i, ^W y_i)^T$ and in antenna frame $(^A x_i, ^A y_i)^T$. The detection area $\mathcal{A}$ is marked in gray.

the position of a RFID tag in the world frame and in the antenna frame. The rotation angle between the antenna frame

and the world frame depends on the heading of the robot (θ) and the constant alignment of the antenna (φ) with respect to the robot frame.

The probability of detecting a tag T_i at a position $z_i = (^A x, ^A y)^T$ inside the detection area $\mathcal{A}$ of the reader is nearly 1 and outside the area it is zero:

$$p(T_i | z_i) \begin{cases} 1 & \text{if } z_i \in \mathcal{A} \\ 0 & \text{else} \end{cases} \qquad (2)$$

False positive readings do not arise, owing to the short range of HF RFID technology. Therefore, the RFID reader can be treated as a binary detector if $z_i \in \mathcal{A}$ or not. All positions z_i that fall in the detection area $\mathcal{A}$ of the reader lead to the same measurement.

A RFID measurement can be interpreted as a *quantized measurement* of a position, which may depend on the headings of the robot. The quantization depends on the size of $\mathcal{A}$ and can be modeled by quantization noise. This interpretation leads to a localization algorithm, which is based on Quantized Kalman filtering [6, 7].

3   Related Works

In order to allow free navigation of mobile robots, some research on RFID localization using a grid of floor-installed RFID tags has been done. Kodaka et al. apply a Particle filter (Sequential Monte Carlo method, MCPF) for pose estimation of a mobile robot using floor based RFID tag and odometry [8]. Mi and Takahashi localize an omnidirectional mobile robot using a RFID system with multiple readers [9]. They compare configurations with different numbers of readers and tag densities [10]. They develop a likelihood function of tag detection which is suitable for localization using MCPF. Main drawback of the MCPF is the computational expense associated with it. Thus, there is some effort to replace the MCPF with methods based on Kalman filtering. Choi et al. propose the fusion of ultrasonic sensors, odometry and readings of HF RFID tags, which are integrated in the floor [11]. This localization algorithm is based on Kalman filtering but needs additional sensors and mapping of the environment. Lee et al. have developed a Gaussian measurement model for UHF RFID tags embedded in the floor, which is suitable for Kalman filtering [12]. Its application in a Kalman filter has less computational expense but provides not the same localization accuracy as a MCPF.

There is also some research on UHF tags at walls or ceilings for self-localization of mobile robots. DiGiampaolo and Martinelli have developed a Quantized Extended Kalman Filter algorithm for localization on mobile robots using UHF RFID tags at the ceiling [13]. Boccadoro et. al. propose a Constrained Kalman filter for global localization of mobile robots using UHF RFID technology and odometry [14]. In that research, the tags are placed at the walls in an indoor environment. Levratti et. al. present a localization algorithm for robotic lawnmowers based on the Constrained Kalman filter proposed in [14]. It merges odometry with UHF RFID tags, which are placed at the borders of the working area [15].

4 Compared Localization Algorithms

This section describes the pose estimation with three different types of estimators. A pose estimator for localization of mobile robots needs a motion model of the mobile robot and a sensor model of its measurements. The compared algorithms are independent of the motion model. For experimental evaluation, we use an omnidirectional mobile robot with Mecanum wheels. The motion model of this mobile robot is described in section 5.3. In this section, the sensor model of RFID readings and the algorithms for measurement updates of the pose estimators are described. A RFID measurement gives the information if a tag T_i with the position t_i is inside or outside the detection area $\mathcal{A}$ of the reader. Beside this binary nature of RFID measurements there are additional sources of uncertainty:

- Communication delay between the RFID reader and the tag: This delay is caused by the limited data rate of the air interface and the collision avoidance procedure for multi tag readings.

- Communication delay between the control system and the RFID reader: This delay is caused by the processing time of the reader and the limited data rate on the interface to the reader.

- Variations in tag placement: Due to production tolerances and manual placement, the position of the RFID tags may differ from the regular grid.

The uncertainty in the tag placement can be treated as Gaussian noise. The communication delays causes additional noise that depends on the speed of the vehicle.

With this additional uncertainty, the measurement function (1) can be extended:

$$z_i = h(x, t_i, v), \qquad (3)$$

where v is the measurement noise caused by communication delays and tag misplacement due to production tolerances. We assume that v is normally distributed with zero mean.

4.1 Sequential Monte Carlo method, Particle Filter (MCPF)

As mentioned before, usually MCPFs are deployed in RFID localization algorithms, because of the highly nonlinear and quantized measurements by RFID readers. A MCPF will be used as benchmark for our proposed localization algorithms.

In the motion update of a MCPF, all particles are sampled with a random generator and distributed through the motion model of the mobile robot. The measurement update in a MCPF is straight forward (see also [8]). After the mobile robot has detected a RFID tag, each particle $x_k^{[m]}$ is distributed through the measurement function $z_i^{[m]} = h(x_k^{[m]}, t_i, 0)$ and then weighted with the associated probability ($p_k^{[m]} = p(z_i^{[m]})$). The measurement noise can be modeled with a normal distribution $v_k \sim \mathcal{N}(0, R_k)$.

Algorithm 1 shows the outline of the MCPF algorithm. Inputs are the particle set $\mathcal{X}_{k-1}$ of the previous time step, the input vector u_k for odometry, the tag measurement vector y_k, and the map with the positions of the RFID tags. The return value is the new particle set $\mathcal{X}_k$ for the actual time step.

Algorithm 1 MCPF

1: **function** MCPF($\mathcal{X}_{k-1}, u_k, y_k, map$)
2:   $\bar{\mathcal{X}}_k = \emptyset$ ▷ initial particle set
3:   **for each** $x_{k-1}^{[m]} \in \mathcal{X}_{k-1}$ **do**
4:     $w_k = sample(u_k)$ ▷ motion noise
5:     $x_k^{[m]} = f(x_{k-1}^{[m]}, u_k, w_k)$ ▷ prediction
6:     $T_i = y_k$ ▷ RFID reader measurement
7:     **if** T_i **then**   ▷ tag detected
8:       $t_i = pos(map, T_i)$ ▷ position of tag in map
9:       $z_i^{[m]} = h(x_k^{[m]}, t_i, 0)$ ▷ pos. in ant. frame
10:      $p_k^{[m]} = p(z_i^{[m]})$ ▷ propability of detection
11:     **else**
12:      $p_k^{[m]} = p(\text{no tag})$ ▷ no measurement
13:     **end if**
14:     $\bar{\mathcal{X}}_k = \bar{\mathcal{X}}_k + < x_k^{[m]}, p_k^{[m]} >$ ▷ insert particle
15:   **end for each**
16:   $\mathcal{X}_k = resample(\bar{\mathcal{X}}_k)$
17:   **return** $\mathcal{X}_k$ ▷ new particle set
18: **end function**

4.2 Quantized Kalman Filtering (QEKF)

In this section, the Quantized Kalman filter we have developed in [6, 7] is summarized. The detection of a tag can be considered as a quantized measurement of a position. The center of the detection area $\mathcal{A}$ defines the position measurement in the antenna frame. The size of $\mathcal{A}$ is a measure of the uncertainty in the measurement and can be modeled as quantization noise. After detecting the tag T_i, the predicted measurement is defined by $\hat{z}_i = h(\hat{x}_k, t_i, 0)$.

The *Gaussian-Fit Algorithm* proposed by Curry [16, p. 23–25] is applied to nonlinear Kalman filtering. The first and second moment of $p(z_i|z_i \in \mathcal{A})$ are needed in the measurement update of a nonlinear KF. For notational convenience let

$$\mu = \mathrm{E}(z_i|z_i \in \mathcal{A}), \ \Sigma = \mathrm{cov}(z_i|z_i \in \mathcal{A}).$$

Mean μ and covariance Σ of the detection area $\mathcal{A}$ can be calculated in advance using numerical integration (see [6]). Additional measurement noise caused by communication delays and tag misplacement due to production tolerances can be modeled with a random variable v_k. It is assumed that $v_k \sim \mathcal{N}(0, R_k)$.

Before the measurement update is performed, the innovation of the measurement T_i is checked. If $\hat{z}_i = h(\hat{x}_k, t_i, 0) \in \mathcal{A}$, the detection of T_i is predicted and the innovation is equal zero. The described algorithm can be applied to the measurement update of any nonlinear Kalman filter. The application of the standard EKF algorithm leads to the algorithm which is shown in **Algorithm** 2, where $H_k = \frac{\partial h}{\partial x}(\hat{x}_k, t_i, 0)$, $V_k = \frac{\partial h}{\partial v}(\hat{x}_k, t_i, 0)$, $\Phi_k = \frac{\partial f}{\partial x}(\hat{x}_k, u_k, 0)$ and $W_k = \frac{\partial f}{\partial w}(\hat{x}_k, u_k, 0)$.

Inputs are the state estimate $\hat{x}_{k-1}$ of the previous time step, the input vector u_k for odometry, the tag measurement vector y_k and the RFID map. The return value is the state estimate $\hat{x}_k$ for the actual time step.

Algorithm 2 Quantized EKF Filter

1: **function** QEKF($\hat{x}_{k-1}, y_k, u_k, map$)
2:    $\hat{x}_k^- = f(\hat{x}_{k-1}, u_k, 0)$ ▷ prediction
3:    $P_k^- = \Phi_k P_{k-1} \Phi_k^T + W_k Q_k W_k^T$
4:    $T_i = y_k$ ▷ RFID reader measurement
5:    **if** T_i **then**   ▷ tag detected
6:       $t_i = pos(map, T_i)$ ▷ position of tag in map
7:       $\hat{z}_i = h(\hat{x}_k^-, t_i, 0)$ ▷ position in antenna frame
8:       **if** $\hat{z}_i \in \mathcal{A}$ **then**
9:          $\Delta y = 0$ ▷ no innovation
10:      **else**
11:         $\Delta y = \mu - \hat{z}_i$ ▷ innovation
12:      **end if**
13:      $K_k = P_k H_k^T \left(H_k P_k H_k^T + V_k (R_k + \Sigma) V_k^T \right)^{-1}$
14:      $\hat{x}_k = \hat{x}_k + K_k \Delta y$
15:      $P_k = (I - K_k H_k) P_k^-$
16:    **else**
17:      $\hat{x}_k = \hat{x}_k^-$ ▷ no measurement
18:      $P_k = P_k^-$
19:    **end if**
20:    **return** $\hat{x}_k, P_k$
21: **end function**

4.3 Quantized Extended Finite Impulse Response (QEFIR) Filtering

In this section a localization algorithm based on EFIR is developed. The algorithm uses a similar approach as we have proposed for the Quantized EKF (QEKF) in the previous section. The EFIR algorithm ignores the noise statistics of the dynamics system, which means, the knowledge of Q_k and R_k is not needed. The only free design parameter of the filter is the horizon of measurements $N = N_{opt}$ for filtering. The fundamental structure of the recursive EFIR algorithm is similar to the EKF, but the EFIR filters the past N measurements $y_{k-N} \cdots y_k$ and inputs $u_{k-N} \cdots u_k$ for every time step k.

For time step $s = k - N - 1$ it needs an initial estimate x_s and the generalized noise power gain G_s, which can be obtained from past measurements by using the mapping matrix (see [1]). For simplification the initial generalized noise power gain can be set to unity $G_s = I$ (see [17]). In our application this simplification does not reduce the localization accuracy.

Algorithm 3 shows the outline of the QEFIR algorithm. Inputs are the input vector u, the tag measurement vector y, an initial pose x_s and the RFID map. The return value is the state estimate $\hat{x}_k$ for the actual time step. $H_l = \frac{\partial h}{\partial x}(\tilde{x}_l, t_i, 0)$, $\Phi_l = \frac{\partial f}{\partial x}(\tilde{x}_l, u_l, 0)$.

The QEFIR estimator needs N past measurements for estimating a pose $\hat{x}_k$. We bootstrap the QEFIR estimator with the Full-Horizon EFIR algorithm until the optimal horizon is reached (see [1]). Another option is the use of the QEKF estimator for bootstrapping the QEFIR algorithm.

Algorithm 3 Quantized EFIR Filter

1: **function** QEFIR(x_s, y, u, map)
2:    $s = k - N - 1; G_s = I, \tilde{x}_s = x_s$
3:    **for** $l = s + 1 : k$ **do**
4:       $\tilde{x}_l^- = f(\tilde{x}_{l-1}, u_l, 0)$ ▷ prediction
5:       $T_i = y_l$ ▷ RFID reader measurement
6:       **if** T_i **then**   ▷ Tag detected
7:          $t_i = pos(map, T_i)$ ▷ position of tag in map
8:          $\tilde{z}_i = h(\tilde{x}_l^-, t_i, 0)$ ▷ pos. in antenna frame
9:          **if** $\tilde{z}_i \in \mathcal{A}$ **then**
10:            $\Delta y = 0$ ▷ no innovation
11:         **else**
12:            $\Delta y = \mu - \tilde{z}_i$ ▷ innovation
13:         **end if**
14:         $G_l = \left(H_l^T H_l + (\Phi_l G_{l-1} \Phi_l^T)^{-1} \right)^{-1}$
15:         $\tilde{x}_l = \tilde{x}_l^- + G_l H_l^T \Delta y$
16:       **else**
17:          $\tilde{x}_l = \tilde{x}_l^-$ ▷ no measurement
18:       **end if**
19:    **end for**
20:    **return** $\hat{x}_k = \tilde{x}_l$ ▷ state estimate at time step k
21: **end function**

---

5 Experimental Setup

5.1 NaviFloor®

The NaviFloor® is a glass fiber reinforcement in which passive HF RFID tags are embedded. The NaviFloor® underlay is shipped in rolls including a map of the RFID tags for simplification of the installation [18]. The NaviFloor® is specially developed for installation beneath artificial flooring. It is pressure-resistant up to 45 N/mm² and withstands even heavy indoor vehicles like fork lift trucks.

We have installed a NaviFloor® in our robotics lab. Figure 1 shows a picture taken during the installation procedure. The RFID tags are installed in a grid of 250 mm. The whole installation includes nearly thousand RFID tags. The tags embedded in the NaviFloor® have a rectangular shape 45 mm × 45 mm. NXP chips I-CODE SLI are integrated in the tags. The tags are compliant to ISO 15693 and communicate in the 13.56 MHz HF band.

5.2 RFID Reader

The reader is a "KTS SRR1356 ShortRange HF Reader" with an external antenna with the rectangular shape 80 mm × 80 mm. We have mounted the reader antenna at a distance of 15 mm to the floor. At this distance, the detection area of the reader has a circular shape with a radius of $R = 100$ mm. For this shape, the first and second moment of $p(z_i | z_i \in \mathcal{A})$ can be calculated as below:

$$\mu = \mathrm{E}(z_i | z_i \in \mathcal{A}) = \begin{pmatrix} 0 \\ 0 \end{pmatrix}, \ \Sigma = \mathrm{cov}(z_i | z_i \in \mathcal{A}) = \begin{pmatrix} \frac{R^2}{4} & 0 \\ 0 & \frac{R^2}{4} \end{pmatrix}.$$

The RFID tags in the floor are placed in a regular grid of 250 mm. Thus, at most one RFID tag can be detected at any moment. The reader antenna is mounted in the center of the vehicles frame.

5.3 Omnidirectional Mobile Robot

This section summarizes the probabilistic motion model of a Mecanum wheeled mobile robot we have developed in [6, 19, 20]. An omnidirectional mobile robot is able to move in any direction and to rotate around its z-axis at the same time. Our mobile robot is equipped with Mecanum
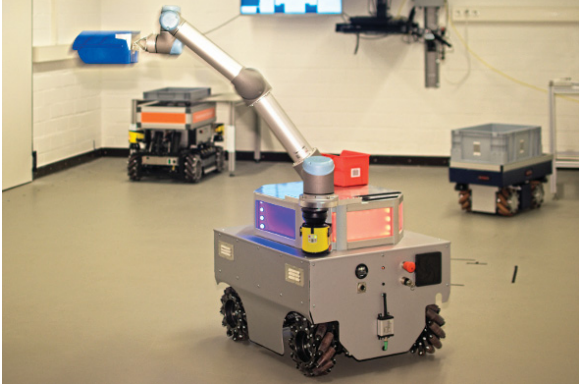

Figure 3 Omnidirectional mobile robots with Mecanum wheels

wheels, which provide three degrees of freedom. Examples of Mecanum wheeled mobile robots in our lab are shown in **Figure 3**. The movements of a mobile robot are corrupted by disturbances caused by mechanical inaccuracies such as unequal floor contact, wheel slippage and inaccuracies in the speed control of the wheels that lead to coupling errors (see [21]). This disturbances will be treated as process noise. Experiments with an omnidirectional mobile robot show that the noise is mainly caused by slippage of the Mecanum wheels. Since the slippage of the wheels depends on the rotational speed of the free spinning rollers, the uncertainty depends on the direction of the movement in the robot frame. Therefore, it is assumed that the movements of the mobile robot in the robot frame are corrupted by independent noise ϵ_i:

$$\Delta \hat{x}_\mathrm{R} = \Delta x_\mathrm{R} + \epsilon_x \,,\ \Delta \hat{y}_\mathrm{R} = \Delta y_\mathrm{R} + \epsilon_y \,,\ \Delta \hat{\theta}_\mathrm{R} = \Delta \theta_\mathrm{R} + \epsilon_\theta \quad (4)$$

Furthermore it is assumed, that the noise ϵ_i is normally distributed with zero mean $\epsilon_i \sim \mathcal{N}(0, \sigma_i^2)$. The standard deviation σ_i is proportional to the displacement in the robot frame and changes in the coupling error $\Delta \varphi_\mathrm{e}$ (see [21]):

$$\begin{pmatrix} \sigma_x \\ \sigma_y \\ \sigma_\theta \end{pmatrix} = \begin{pmatrix} \alpha_x^x & \alpha_x^y & \alpha_x^\theta & \alpha_x^\mathrm{e} \\ \alpha_y^x & \alpha_y^y & \alpha_y^\theta & \alpha_y^\mathrm{e} \\ \alpha_\theta^x & \alpha_\theta^y & \alpha_\theta^\theta & \alpha_\theta^\mathrm{e} \end{pmatrix} \cdot \begin{pmatrix} \Delta x_\mathrm{R} \\ \Delta y_\mathrm{R} \\ \Delta \theta_\mathrm{R} \\ \Delta \varphi_\mathrm{e} \end{pmatrix} \quad (5)$$

The parameters α_i^j are robot-specific constants, which can be identified by experiments. With the additional noise, the motion model can be described as follows:

$$\boldsymbol{x}_k = \boldsymbol{f}(\boldsymbol{x}_{k-1}, \boldsymbol{u}_k, \boldsymbol{w}_k), \quad \text{with} \quad \boldsymbol{x}_k = \begin{pmatrix} x_k \\ y_k \\ \theta_k \end{pmatrix}, \quad (6)$$

$$\boldsymbol{u}_k = \begin{pmatrix} \Delta x_\mathrm{R} \\ \Delta y_\mathrm{R} \\ \Delta \theta_\mathrm{R} \\ \Delta \varphi_\mathrm{e} \end{pmatrix}, \quad \boldsymbol{w}_k = \begin{pmatrix} \epsilon_x \\ \epsilon_y \\ \epsilon_\theta \end{pmatrix}$$

where $\boldsymbol{u}_k$ is obtained by odometry using wheel encoder measurements (see [6]).

$$\begin{aligned} x_k &= x_{k-1} + (\Delta x_\mathrm{R} + \epsilon_x) \cos\left(\theta_{k-1} + \tfrac{\Delta\theta + \epsilon_\theta}{2}\right) \\ &\quad - (\Delta y_\mathrm{R} + \epsilon_y) \sin\left(\theta_{k-1} + \tfrac{\Delta\theta + \epsilon_\theta}{2}\right) \\ y_k &= y_{k-1} + (\Delta x_\mathrm{R} + \epsilon_x) \sin\left(\theta_{k-1} + \tfrac{\Delta\theta + \epsilon_\theta}{2}\right) \\ &\quad + (\Delta y_\mathrm{R} + \epsilon_y) \cos\left(\theta_{k-1} + \tfrac{\Delta\theta + \epsilon_\theta}{2}\right) \\ \theta_k &= \theta_{k-1} + \Delta\theta + \epsilon_\theta \end{aligned} \quad (7)$$

In the prediction step of the EKF, the estimated pose of the robot

$$\hat{\boldsymbol{x}}_k = \boldsymbol{f}(\hat{\boldsymbol{x}}_{k-1}, \boldsymbol{u}_k, \boldsymbol{0}) \quad (8)$$

and the covariance of the pose

$$\boldsymbol{P}_k = \boldsymbol{\Phi}_k \boldsymbol{P}_{k-1} \boldsymbol{\Phi}_k^\mathrm{T} + \boldsymbol{W}_k \boldsymbol{Q}_k \boldsymbol{W}_k^\mathrm{T}, \quad (9)$$

can be calculated based on $\boldsymbol{f}(\cdot)$ and its Jacobians $\boldsymbol{\Phi}_k$ and $\boldsymbol{W}_k$:

$$\boldsymbol{\Phi}_k = \frac{\partial \boldsymbol{f}}{\partial \boldsymbol{x}}(\hat{\boldsymbol{x}}_k, \boldsymbol{u}_k, \boldsymbol{0}) \quad \text{and} \quad \boldsymbol{W}_k = \frac{\partial \boldsymbol{f}}{\partial \boldsymbol{w}}(\hat{\boldsymbol{x}}_k, \boldsymbol{u}_k, \boldsymbol{0}) \quad (10)$$

The process covariance matrix

$$\boldsymbol{Q}_k = \begin{pmatrix} \sigma_x^2 & 0 & 0 \\ 0 & \sigma_y^2 & 0 \\ 0 & 0 & \sigma_\theta^2 \end{pmatrix} \quad (11)$$

can be calculated using (5).

6 Experimental Results

We have conducted several experiments with an omnidirectional mobile robot over an array of floor installed HF RFID tags [7]. The measurements of the RFID reader and the wheel encoders are stored in a file and evaluated off-line with Matlab.

Figure 4 shows the estimated trajectories of one of these experiments. The mobile robot moves a square path clockwise from the starting point at the left side of the figure to the end point in the lower left corner. The path is transverse to the grid with an angle of 5°. Global localization of the mobile robot is realized as we have proposed in [7].

In Figure 4, RFID tags that are detected by the reader are shown as black circles. Since the antenna in mounted in the center of the robot frame and the shape of the detection area is circular, the printed circles are the projection of the detection area onto the working plane.

The pose estimation is started right after the second RFID tag is detected ($x = 2000\,\mathrm{mm}$, $y = 5750\,\mathrm{mm}$). Due to the quantized measurements, the localization error is large at the beginning of the path and becomes smaller while moving. Hence, after global localization, the estimated heading is parallel to the grid ($\hat{\theta} = 90°$). After detecting additional tags, all filters correct the estimated heading and therefore the direction of movement. The magenta curve in Figure 4 shows, that the MCPF needs the least way length to correct the misalignment. The Quantized EKF (QEKF, green curve) tend to force the position estimate into direction of
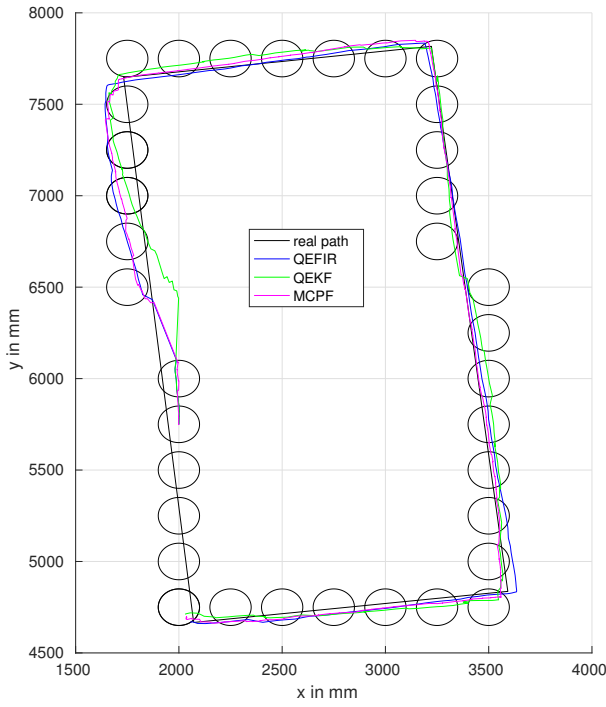
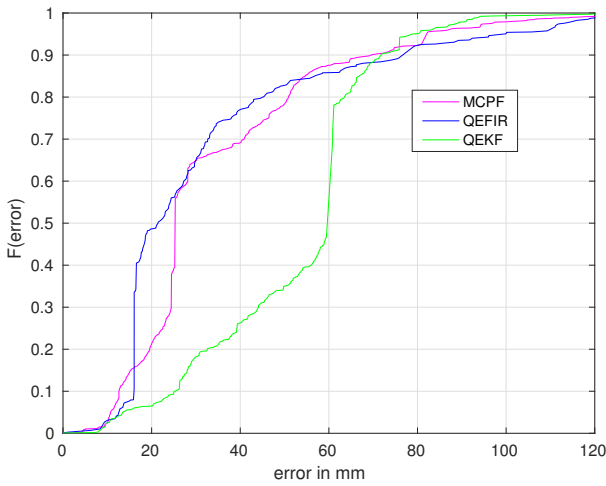**Figure 4** Estimated trajectories of QEFIR, MCPF and QEKF

Figure 5 Cumulative Distribution Function (CDF) of localization errors

the center of detected tags. The Quantized EFIR (QEFIR, blue curve) is able to follow the real path with a smaller deviation than the QEKF.

Figure 5 compares the Cumulative Distribution Function (CDF) of the pose estimators for this experiment. The figure shows that the application of the QEFIR leads to a similar localization performance than the MCPF and a better performance than the QEKF. Compared to the QEKF, the QEFIR needs more computations for every time step and is able to run in real-time on fast computers only. The MCPF needs even more computations and is not able to run in real-time and serves as a benchmark only. The location performance of the compared estimators depends on the trajectory and is different for each experiment, which we have evaluated. Normally, the location accuracy of the
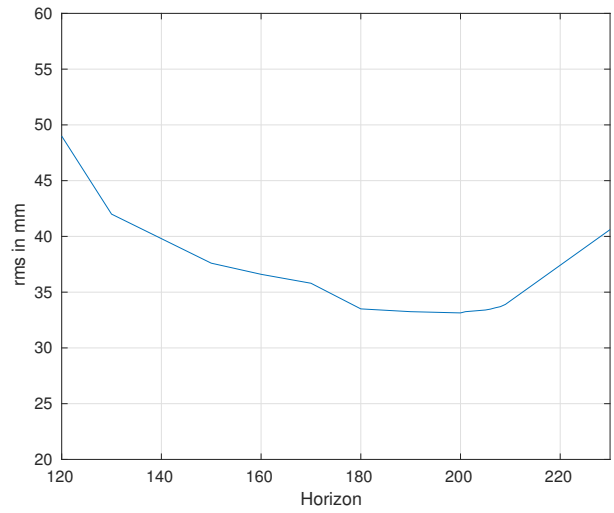

Figure 6 Optimal horizon of QEFIR filtering

QEFIR estimator is similar or better than the QEKF algorithm, but there are also a few cases, where the accuracy of the QEFIR is lower than the accuracy of the QEKF.

Figure 6 compares the localization accuracy of the QEFIR algorithm for different horizons N_{opt}. The optimal horizon is found at $N_{opt} \approx 200$ experimentally with the trajectory shown in Figure 4. A smaller as well as a larger horizon decreases the localization accuracy. The computational expanse increases linearly with the horizon.

7 Conclusions

In this paper, we have presented a novel localization algorithm based on the EFIR algorithm that fuses sensory data from wheel encoders with RFID readings. The RFID readings are assumed as quantized measurement of the robot's position. This assumption considers the binary nature of floor-installed HF RFID tags. In many cases, the localization accuracy of the Quantized EFIR algorithm is similar to the MCPF but with much less computational expense. The QEFIR estimator outperforms the QEKF algorithm, if the horizon of measurements is optimal. Compared to the QEKF, the QEFIR needs more computations for every time step and is able to run in real-time on fast computers only. The accuracy of the localization method is sufficient for most industrial applications.

The localization concept is suitable for small and inexpensive mobile robots, since the robots must be equipped with an inexpensive and small HF RFID reader only. Compared to localization using laser range finders as position sensor, a HF RFID reader is much cheaper. Compared to localization using optical or inductive guidance, localization using a grid of floor-installed tags is more flexible. The installation of the RFID infrastructure causes the highest expense for this localization method, but since passive RFID technology is used, the infrastructure is free of maintenance costs.

8   Literature

[1] Y. S. Shmaliy, S. Zhao, and C. K. Ahn. Unbiased finite impulse response filtering: An iterative alternative to Kalman filtering ignoring noise and initial conditions. *IEEE Control Systems*, 37(5):70–89, Oct 2017.

[2] E. Guizzo. Three Engineers, Hundreds of Robots, one Warehouse. *IEEE Spectrum*, 7:27–34, 2008.

[3] Guidong Liu, Wensheng Yu, and Yu Liu. Resource management with RFID technology in automatic warehouse system. In *Intelligent Robots and Systems, 2006 IEEE/RSJ International Conference on*, pages 3706–3711, 2006.

[4] Götting KG. Introduction transponder positioning. http://www.goetting-agv.com/components/transponder/introduction.

[5] M. Baum, B. Niemann, and L. Overmeyer. Passive 13.56 MHz RFID transponders for vehicle navigation and lane guidance. In *Proceedings of the 1st International EUR AS IP Workshop on RFID Technology*, pages 83–86, 2007.

[6] C. Röhrig, A. Heller, D. Heß, and F. Künemund. Global localization and position tracking of automatic guided vehicles using passive RFID technology. In *Proceedings of the joint 45th International Symposium on Robotics (ISR 2014) and the 8th German Conference on Robotics (ROBOTIK2014)*, Munich, Germany, June 2014.

[7] C. Röhrig, D. Heß, and F. Künemund. Constrained Kalman filtering for indoor localization of transport vehicles using floor-installed HF RFID transponders. In *Proceedings of the 9th Annual IEEE International Conference on RFID (IEEE RFID 2015)*, pages 113–120, San Diego, CA USA, April 2015.

[8] K. Kodaka, H. Niwa, Y. Sakamoto, M. Otake, Y. Kanemori, and S. Sugano. Pose estimation of a mobile robot on a lattice of RFID tags. In *Intelligent Robots and Systems, 2008. IROS 2008. IEEE/RSJ International Conference on*, pages 1385–1390, 2008.

[9] J. Mi and Y. Takahashi. Performance analysis of mobile robot self-localization based on different configurations of rfid system. In *Proceedings of the 2015 IEEE International Conference on Advanced Intelligent Mechatronics (AIM)*, pages 1591–1596. IEEE, July 2015.

[10] Jian Mi and Yasutake Takahashi. Low cost design of hf-band rfid system for mobile robot self-localization based on multiple readers and tags. In *Proceedings of the 2015 IEEE International Conference on Robotics and Biomimetics (ROBIO)*, pages 194–199. IEEE, Dec 2015.

[11] Byoung-Suk Choi, Joon-Woo Lee, Ju-Jang Lee, and Kyoung-Taik Park. A hierarchical algorithm for indoor mobile robot localization using RFID sensor fusion. *Industrial Electronics, IEEE Transactions on*, 58(6):2226–2235, 2011.

[12] Jewon Lee, Youngsu Park, Daehyun Kim, Minho Choi, Taedong Goh, and Sang-Woo Kim. An efficient localization method using RFID tag floor localization and dead reckoning. In *Control, Automation and Systems (ICCAS), 2012 12th International Conference on*, pages 1452–1456, 2012.

[13] Emidio DiGiampaolo and Francesco Martinelli. A passive UHF-RFID system for the localization of an indoor autonomous vehicle. *Industrial Electronics, IEEE Transactions on*, 59(10):3961–3970, 2012.

[14] Mauro Boccadoro, Francesco Martinelli, and Stefano Pagnottelli. Constrained and quantized kalman filtering for an RFID robot localization problem. *Autonomous Robots*, 29(3-4):235–251, 2010.

[15] Alessio Levratti, Matteo Bonaiuti, Cristian Secchi, and Cesare Fantuzzi. An inertial/RFID based localization method for autonomous lawnmowers. In *Proceedings of the 10th IFAC Symposium on Robot Control, IFAC SYROCO 2012*, pages 145–150, Dubrovnik, Croatia, September 2012.

[16] Renwick E. Curry. *Estimation and Control with Quantized Measurements*. MIT Press Cambridge, 1970.

[17] J. J. Pomárico-Franquiz, M. Granados-Cruz, and Y. S. Shmaliy. Self-localization over RFID tag grid excess channels using extended filtering techniques. *IEEE Journal of Selected Topics in Signal Processing*, 9(2):229–238, March 2015.

[18] A. Steinhage and C. Lauterbach. SensFloor® and NaviFloor®: Large-area sensor systems beneath your feet. In N. Chong and F. Mastrogiovanni, editors, *Handbook of Research on Ambient Intelligence and Smart Environments: Trends and Perspectives*, pages 41–55. Hershey, PA: Information Science Reference, 2011.

[19] C. Röhrig, D. Heß, C. Kirsch, and F. Künemund. Localization of an Omnidirectional Transport Robot Using IEEE 802.15.4a Ranging and Laser Range Finder. In *Proceedings of the 2010 IEEE/RSJ International Conference on Intelligent Robots and Systems (IROS 2010)*, pages 3798–3803, Taipei, Taiwan, October 2010.

[20] D. Heß, F. Künemund, and C. Röhrig. Simultaneous calibration of odometry and external sensors of omnidirectional automated guided vehicles (AGVs). In *Proceedings of the 47th International Symposium on Robotics (ISR 2016)*, pages 480–487, Munich, Germany, June 2016.

[21] C. Röhrig, D. Heß, and F. Künemund. Motion controller design for a mecanum wheeled mobile manipulator. In *Proceedings of the IEEE Conference on Control Technology and Applications (CCTA 2017)*, pages 444–449, Kohala Coast, Hawai'i, USA, August 2017.